Diamond & Related Materials 119 (2021) 108585

Contents lists available at ScienceDirect

Diamond & Related Materials

journal homepage: www.elsevier.com/locate/diamond

The effects of the CNF ratio on the microstructure, corrosion, and mechanical properties of CNF-reinforced diamond cutting tool

Serkan Islak [a,*], Cihan Özorak [b], Naser Matoug Emhmed Abouacha [c], Uğur Çalıgülü [d], Vahdettin Koç [e], Özkan Küçük [f]

[a] Kastamonu University, Faculty of Engineering and Architecture, Department of Mechanical Engineering, Kastamonu, Turkey
[b] Kastamonu University, Faculty of Engineering and Architecture, Department of Metallurgy and Materials Engineering, Kastamonu, Turkey
[c] Kastamonu University, Institute of Science, Kastamonu, Turkey
[d] Fırat University, Faculty of Technology, Department of Metallurgy and Materials Engineering, Elazığ, Turkey
[e] Adıyaman University, Vocational High School of Technical Sciences, Adıyaman, Turkey
[f] Bilecik Şeyh Edebali University, Faculty of Engineering, Department of Metallurgy and Materials Engineering, Bilecik, Turkey

ARTICLE INFO

Keywords:
CNF
Bronze
Diamond cutting tools
Microstructure
Mechanical property
Corrosion

ABSTRACT

This study sets out to investigate the effects of CNF on the microstructure, corrosion, and mechanical properties of a carbon nanofiber (CNF)-reinforced diamond cutting tool matrix. First, CNF was added to bronze (i.e. the matrix) at different ratios (0, 0.25, 0.50, 0.75, and 1.00 wt%). Hot pressing was selected as the preferred method of production as it allows producing a larger number of compact samples. Next, the manufactured samples' microstructure, hardness, density, transverse rupture strength (TRS), corrosion, and wear properties were analysed. Then, their microstructures and phase compositions were examined using optical microscopy and XRD. Their hardness was measured using a microhardness device. Their TRS values were calculated using a three-point bending test. Their fractured surfaces were examined using SEM-EDS. Wear properties were examined using the reciprocating wear test. Their corrosion behaviours were analysed using potentiodynamic measurements. Optical microscope images showed that CNF exhibited flocculation in several areas along the bronze matrix. The samples' hardness increased significantly with higher CNF ratios, whereas their relative densities dropped slightly. The TRS reached its maximum value at 0.25% CNF. Beyond that, a significant drop was observed in TRS. The higher the samples' CNF ratios were, the less corrosion resistance they got due to the microgalvanic effect. The results of wear test showed that as the samples' CNF ratios rose, their wear rates and their friction coefficients incrementally dropped.

1. Introduction

Processing natural stones in a high quality manner – and without any waste – is a vital issue in this century, for how we use our natural resources is of crucial importance. This highlights the continuous development of diamond cutting tools. Most studies in the literature deal with the development of cutting tool matrix. A matrix is expected both to grasp the diamond grain tightly when cutting natural stone and to wear in a convenient manner. If a matrix fails to wear down, the diamond will become blunt during the cutting process, thus damaging the tool. However, if the matrix wears in an optimal manner, it will release blunt and broken diamond particles. Moreover, new diamond particles will appear on the lower part of the matrix, thereby allowing the cutting process to continue [1,2].

Tool manufacturers widely use bronze, nickel, cobalt, iron, and their respective alloys when making cutting tool matrix. Scientists are working hard on these matrices. Most of these are the development of alternative matrices to cobalt. Chen et al. [3] studied the production and characterization of CuNiSn-Al_2O_3 composite matrix, which can be an alternative to cobalt. As a result of the studies, it was concluded that the CuNiSn-Al_2O_3 matrix is cheaper and has a longer service life than cobalt. Su et al. [4] studied the cutting efficiency of the diamond cutting tool of nickel-coated graphite added to Fe at different rates. It has been reported that there is an increase in the service life of the cutting tool with the addition of graphite, and it can also be used for cutting natural stones with hard minerals. Hu et al. [5] studied the usability of pre-alloyed Fe-

* Corresponding author at: Kastamonu University, Faculty of Engineering and Architecture, Department of Mechanical Engineering, 37150 Kastamonu, Turkey.
E-mail address: serkan@kastamonu.edu.tr (S. Islak).

https://doi.org/10.1016/j.diamond.2021.108585
Received 6 July 2021; Received in revised form 6 August 2021; Accepted 23 August 2021
Available online 27 August 2021

based and Cr-Fe-based diamond drills instead of WC-containing drills. As a result of the drilling experiments, it was emphasized that these matrix designs can replace the WC-containing drills. Soltani and Tayebi [6] studied on the determination of wear parameters and mechanisms of diamond/copper tools in marble cutting. They used a composition of 78% brass (Cu—10Zn) + 16% bronze (Cu—10Sn) + 6%Co. The effect of different wear mechanisms on the metal binder and diamond grains of the cutting tool was evaluated by cutting a very hard type of marble stone called Cappochino Beige Marble. According to the low hardness of the cutting tool and the wear in the matrix, the life of the cutting tool was low, but the cutting rate was quite high. Cygan-Bączek et al. [7] developed a SiC, Al_2O_3 and ZrO_2 reinforced diamond cutting tool matrix with Fe-Mn-Cu-Sn matrix. This new matrix produced was compared with the cobalt-based matrix in terms of mechanical properties. According to their results, it has been reported that the newly produced matrix is harder and more wear-resistant than the cobalt-based matrix. Çelik and Aslan [8] produced a powder mixture of Cu-Fe-Co using hot pressing method to improve the bonding between diamond and matrix. It was observed that the porosity ratios of the hot pressed samples decreased with the increase in temperature and pressing parameters. It was observed that Cu diffuses in the matrix and fills the micropores. It was determined that hardness values decreased as a result of grain growth after heat treatment. Çelik [9] produced the FeCuNiSnPMoMn alloy matrix by mechanical alloying followed by hot pressing, due to the harmful effects and cost of cobalt. As a result of the experimental data obtained, it was observed that as the hot pressing temperature increased, the porosity ratio in the samples decreased and the transverse rupture strength increased up to 1446 MPa. Within the framework of these results, it was concluded that the Fe-based matrix could be used as an alternative to Co in the diamond cutting tool industry. Li et al. [10] investigated the mechanical properties of Cu-Fe-Co matrices for diamond cutting tools. In order to reduce the cobalt ratio in the study, the samples were produced by vacuum and pressure sintering process. The results showed that the density, hardness and strength were higher at high sintering temperature (820 °C) than at low temperature (740 °C). The matrix densification elevation and diffuse dispersion of Co—Cr pre-alloyed powders contributed to a hardness improvement and tensile strength improvement to the Cu-Fe-based matrix. Bulut et al. [11] studied the determination of the matrix composition for diamond cutting tools according to the hardness and abrasiveness of the rocks to be cut. Two metal matrix compositions based on Co and Fe were selected and their microstructures, mechanical properties and wear properties were investigated comparatively. The results showed that the mechanical properties of different matrix composition, hardness and wear resistance of Co-based matrices are higher than Fe-based matrices. It has been reported that Fe-based matrix is more suitable for cutting marble, while Co-based matrix is more suitable for cutting granite. Çelik et al. [12] developed Fe-10Cu-1Al_2O_3-xMo matrix as an alternative to cobalt. They discovered that the hardness and bending strength of the matrix increased depending upon the molybdenum ratio. They ultimately concluded that these matrices are possible candidates for the diamond cutting tool matrix. Scientists have also adapted the materials they have developed in the field of materials for diamond cutting tool matrix. For example, Zhang et al. [13] developed FeCoCrNiMo high-entropy alloys (HEAs) using powder metallurgy for diamond cutting tool applications. FeCoCrNiMo HEAs have considerably higher hardness and exhibit better wear behaviour than metal matrix utilised in common diamond tools, thus meaning that they can also be used in diamond cutting tools. Zeren and Karagöz [14] used cobalt and nickel as matrix and various amounts of bronze as filling material. They characterized the microstructure of diamond cutting tool by two main properties: diamond and matrix. They firmly supported the matrix to prevent them from becoming damaged during cutting. They reported that the bonding between matrix and diamond should be strong enough to yield high performance. Kir et al. [15] and Islak et al. [16] studied the usability of cubic boron nitride (cBN) as an alternative to diamond. In this study, bronze (Cu—Sn) matrix, which is frequently used in the cutting tool industry, was preferred. As a result of this study, it was concluded that cBN can be used instead of diamond, but its service life is low. Islak and Çelik [17] investigated the effect of production parameters on the cutting performance of the composite matrix by adding boron carbide (B_4C) to the bronze matrix in diamond cutter technology. It has been reported that optimum cutting performance is achieved at a sintering temperature of 700 °C and a ratio of 5% B_4C. The matrix needs to wear optimally against hard natural stone. This necessitates the development of many matrices mentioned above. However, in these studies, while trying to increase the hardness, the porosity also increases. This situation causes breakage during cutting with the tool. This pushes scientists to look for different matrices.

Numerous studies have reported that nano reinforcements have a number of positive effects on many properties of composite materials [18–20]. However, the use of nanotechnology in cutting tool technologies is limited at present. Diamond cutting tools with higher strength and lower porosity can be produced using nano-sized particles/fibers. The aim of this study is to produce diamond cutting tools via hot pressing method by adding carbon nanofibers to the diamond cutting tool matrix at different ratios and to examine the microstructure, wear, and corrosion properties of the cutting tools produced.

2. Experimental studies

Bronze powder was used as a matrix, whereas carbon nanofiber (CNF) was used as matrix reinforcing element. Synthetic diamond was also added to the matrix so that the researchers could determine the diamond retention properties of the matrix. Bronze alloy containing 85% Cu and 15% Sn was used; the average particle diameter was 30 μm. Sigma Aldrich CNF that was 100-nm in diameter and a 20–200 μm long was used as a matrix reinforcing element. Table 1 illustrates the properties of the powders used to manufacture the samples. Fig. 1 shows the powders' SEM-EDS and XRD analyses. Bronze powder grains were spherical, whereas CNF powder grains resembled fiber. Diamond particles had a cubic octahedral structure. According to the XRD analysis of the powders, the bronze powder was composed of α-Cu and Ɛ-bronze (Cu_3Sn) phases. The graph clearly shows that only phase C occurred a peak in the XRD analysis of CNF. These formations were the expected phase formations. According to the EDS analysis, bronze powder contained Cu and Sn, CNF contained C, and the diamond was composed of Ti and C. Ti represents the diamond's external coating.

A three-axis rotary mixer was employed to achieve a homogeneous dispersion of the said powders. First, CNF at different ratios was added into the bronze powder (Table 2). Next, PEG (polyethylene glycol) of 1 wt% was added to the powder mixture to ensure the powders blended well, and to prevent flocculation. They were then mixed with chrome coated steel balls at 20 rpm for 20 min. Synthetic diamond was also added to this mixture to produce three-point bending test samples. Diamond and diamond-free mixtures mixed in the powder mixer were pressed in a cold pressing machine. Then, the cold-pressed samples were put in graphite moulds. Afterwards, a socket-loaded graphite mould block – prepared for sintering – was placed in the hot pressing area. The mould block was placed in a hot pressing machine and hot pressed under 35 MPa at 680 °C for 4 min. The whole process was carried out in a PLC-control vacuum hot press machine (Zhengzhou Golden Highway, SMVB 80, China) (Fig. 2).

Table 1
The properties of the powders used in the production of the samples.

Properties	Powders		
	Bronze	CNF	Diamond
Particle size	~30 μm	D × L 100 nm × 20–200 μm	40/50 mesh
Purity (%)	99	>98	99

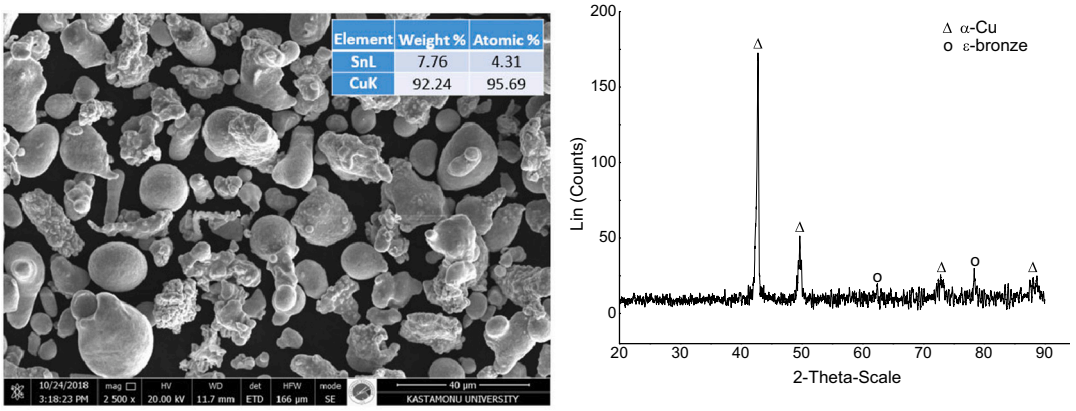

(a)

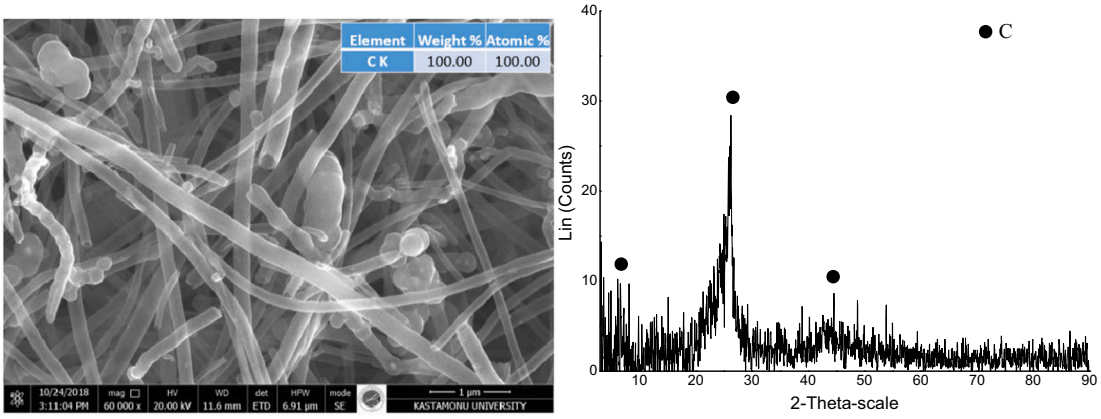

(b)

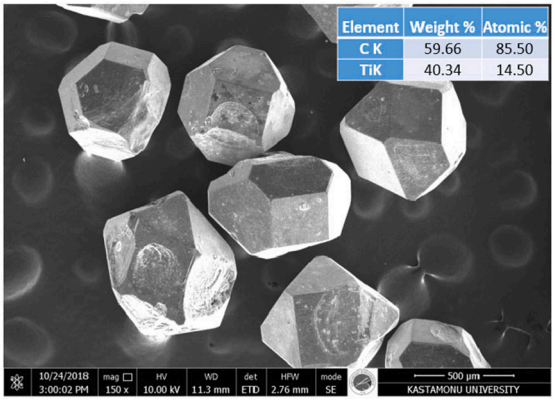

(c)

Fig. 1. SEM images and XRD analysis of the samples: (a) bronze and (b) CNF and (c) diamond.

First, the surfaces of all of the samples were sanded with 320–1200 mesh sandpaper. Then, the surfaces of the samples were polished with 1- and 6-mm diamond paste and thinner. Then, the samples were etched in 5 g. $FeCl_3$ + 50 ml HCl + 100 ml H_2O solution for 20 s. An Olympus GX41 inverted metallurgical microscope, a stream image analysis system, a scanning electron microscope (FEI QUANTA 250 FEG), energy dispersive spectroscopy (EDS), and X-ray diffraction (Bruker D8 Advance) were used to examine the microstructure of the samples, appoint their phase structures, and interpret their fracture surfaces. The hardness of the samples was measured before using SHIMADZU HMV-G21 micro hardness tester.

The hardness of each sample was calculated from its different surfaces (diamond-free samples) as a total of 10 values under a load of 1 kg for 15 s. The evaluation was made by calculating the average of all of the values. The densities of the sample were calculated using Quantachrome Ultrapyc 1200E helium pycnometer. Relative densities of the samples were found by dividing the experimental densities (detected using the helium pycnometer) by the calculated theoretical density.

The three-point bending test was carried out at a speed of 1 mm/min on Shimadzu AG-IC universal tensile testing machine (50 kN) to determine each sample's transverse rupture strength. Corrosion tests were carried out on a Reference 3000 Potentiostat/Galvanostat/ZRA device.

Table 2
Powder mixture rates and sintering parameters.

Sample no	Matrix (wt%)		Hot pressing parameters			Diamond concentration[a]
	Bronze	CNF	Temperature (°C)	Period (minute)	Pressure (MPa)	
1	100	–	680	4	35	20
2	99.75	0.25	680	4	35	20
3	99.50	0.50	680	4	35	20
4	99.25	0.75	680	4	35	20
5	99.00	1.00	680	4	35	20

[a] 4.4 carat diamond is accepted as 100% for 1 cm^3 socket volume as diamond concentration.

Fig. 2. Hot pressing machine.

The samples were cleaned ultrasonically at 35 °C in acetone for 15 min, distilled water for 15 min, and ethanol for 15 min, and then they were dried in a drying oven at 60 °C for 45 min. Afterwards, they were kept in a 3.5 wt% NaCl solution for approximately 1 h to stabilise them. The current density as well as corrosion potential, corrosion current, and corrosion rate were found by looking at the potential curves. Three experiments were carried out on each sample. New solution was used during each experiment. Then, arithmetic average of the results was calculated. Corrosion current density, corrosion potential, and corrosion rate were calculated directly from the curves by reading the device. All of the samples were subjected to reciprocating wear test on a UTS Tribometer T10 test device (in accordance with ASTM G133 standard) under a load of 10 N at a sliding distance of 350 m (under room conditions). The data collection rate was set to 3 Hz. Ø6-mm-diameter spherical steel balls (made of 100Cr6) were used as abrasive balls. They were replaced for each experiment. The chemical composition and wear surfaces' morphology were analysed using SEM and EDS.

3. Results and discussion

Fig. 3 shows the samples' optical images. The samples were not porous. The addition amount of CNF rose visually the more CNF was added to the samples. However, CNF aggregated in some areas of the bronze matrix. This was due to the fact that the CNF was nano-scaled. CNFs were located along the contact areas of the grains in the bronze matrix. Fig. 4 shows SEM-EDS analysis of the sample containing 0.50% CNF. As mentioned above, the CNFs between the bronze grains were clearly visible. Cu, Sn, and C were detected in the EDS analysis of zone 1. This indicates that C was also present in the lower layers of the matrix. 100% C was present in EDS analysis of zone 2. This zone was completely carbon nanofiber.

Fig. 5 includes graphs of XRD analysis to find out whether a phase formed to ensure bonding at interface between the matrix and CNF. According to the XRD graphs, α-Cu and Cu_3Sn phases formed in the non-reinforced bronze matrix. This was the same as the XRD analysis of the powder before it was hot pressed. The lack of difference between the two situations stemmed from the fact that the matrix powder was an alloy. Had Cu and Sn in bronze been added separately and there would have been a difference in the XRD analysis. When CNF was added, the C peak representing CNF in the XRD graph was detected at the angle of $2\theta = 26.15$. The peak C was not detected in samples manufactured using 0.25% and 0.50% CNF reinforcements. This is either because the reinforcement ratio of CNF was very low or the dispersion was partially homogeneous. However, the peak C was detected in both 0.75% and 1.0% CNF reinforcements. In fact, their peak intensities significantly rose as CNF ratios increased from 0.75 to 1.0. No chemical phase formed between bronze and CNF. No oxide formation occurred in the samples.

Table 3 shows experimental densities measured using helium pycnometry, calculated theoretical densities, and calculated relative densities. The densities were found to change little because of low reinforcement ratio of CNFs. There was not much change in their relative densities. It is worth noting that a limited number of pores formed at higher relative densities.

Fig. 6 shows hardness of the samples. The hardness values of bronze matrix with 0, 0.25, 0.50, 0.75 and 1.0% CNF reinforcements were 174 HV_1, 176 HV_1, 191 HV_1, 201 HV_1 and 210 HV_1, respectively. This indicates a significant increase in the hardness of the samples with higher CNF reinforcement ratio. Hardness of the sample containing 1.0% CNF increased by approximately 21% compared to the hardness of non-reinforced bronze matrix. Here, CNFs prevented the movement of dislocations and resulted in greater hardness. Lim et al. [18] discovered in their study that CNFs increased hardness by preventing the movement of dislocations.

Fig. 7 shows the analysis of the three-point bending data to determine the transverse rupture strength of the samples and detect microstructurally the matrix's synthetic diamond retention capability. This graph shows transverse rupture strengths as a function of the heightened ratio of the carbon nanofibers. In 0, 0.25, 0.50, 0.75 and 1.0% CNF reinforcements, the transverse rupture strengths of the samples were 447.975 MPa, 462.309 MPa, 453.061 MPa, 436.542 MPa and 364.212 MPa, respectively. These values tended to rise in the reinforcement of 0.25% CNF, but to drop as from this value.

This drop in transverse rupture strengths at the reinforcement ratios after 0.25% CNF is associated with the partial clustering of CNFs within the matrix. This may be because the carbon nanofibers clustered together and acted as large grains. When nanoparticles or fibers alone are dispersed homogeneously, they increase strength by filling the pores forming within the material (a result of powder metallurgy). When clustering occurs, those nanoparticles/fibers cannot do these filling functions. Clustered CNFs are more present in the matrix. A cross-sectional weakening occurs in the matrix, thus resulting in a weakened transverse rupture strength. In addition, clustered CNFs lead more pores to form in the matrix, which in turn also weaken the transverse rupture strength [21].

Fig. 8 shows the SEM image of the fracture surface of the CNF non-

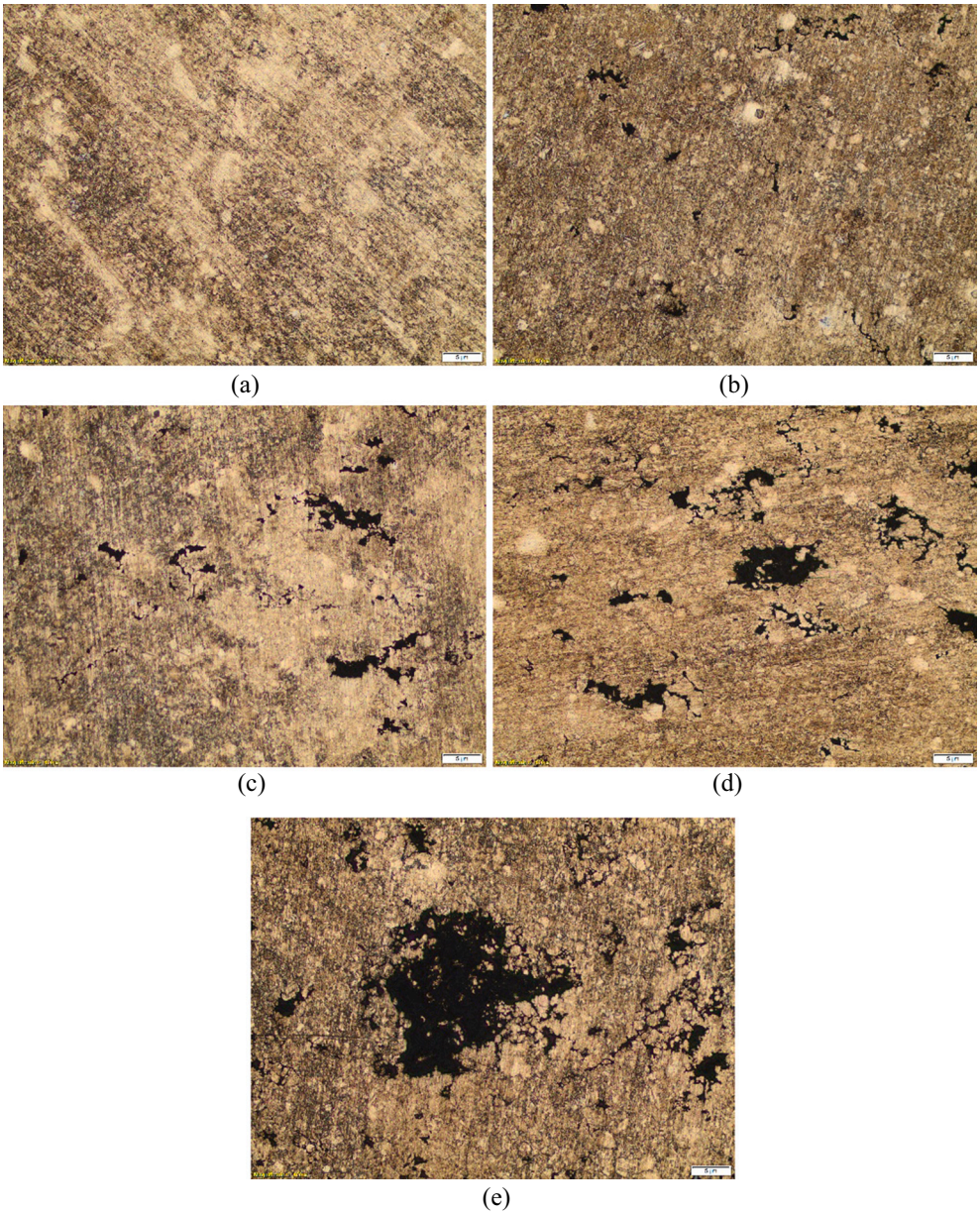

Fig. 3. Optical images: (a) bronze, (b) bronze- 0.25% CNF and (c) bronze- 0.50% CNF, (d) bronze-0.75% CNF and (e) bronze- 1% CNF.

reinforced sample (bronze-diamond). Fig. 8(a) shows the general view (small magnification) of the bronze-diamond sample, while Fig. 8(b) shows the retention of the diamond by the bronze matrix at larger magnification. In Fig. 8(a), diamond housings where diamonds dislocate at the time of fracture were clearly visible. In Fig. 8(b), the diamond particles maintained their physical integrity after the three-point bending test. This is crucial for the diamond cutting tools to carry out their cutting function properly [22]. Fig. 9 shows EDS analysis for non-reinforced bronze-diamond sample. An EDS was taken of the diamond particles in zone 1, and of the matrix in zone 2. Carbon represents the diamonds in the EDS analysis. Titanium represents the titanium coating on the diamond surface. The Ti coating created a strong interface bond between the matrix and the diamond by making it wetter [23].

Among the existing techniques available to strengthen the bonding between the diamonds and the matrix, coating techniques – by which some carbide-forming elements are coated on diamond crystals before being blended with matrix powders – have been found to be highly effective [24,25]. Furthermore, the external coating of diamond prevents it from turning into graphite during sintering. The presence of oxygen in EDS analysis in zone 1 may be due to the oxidation of titanium. The EDS analysis of zone 2 represents the bronze matrix completely.

Fig. 10 includes the SEM images taken of the fracture surfaces of the bronze-0.25% CNF-diamond sample. Based on these images the diamond particles in the 0.25% CNF sample were tightly held together compared to the non-reinforced sample. Moreover, secondary cracks from the image formed on the fracture surface. The formation of these secondary cracks may be caused by the Cu_3Sn phase formed by the tin in the bronze with the copper and/or the CNF reinforced in the matrix. CNFs were not clearly visible in the microstructure of fracture surfaces at low magnifications since their sizes were small, and their reinforcement ratio was low.

Fig. 11 shows SEM images of fracture surfaces of 0.50% CNF, 0.75% CNF, and 1.0% CNF-reinforced bronze-CNF-diamond samples. The images show that the diamond retention capacity of the matrix decreased. Fractures occurred mostly in the form of intergranular separation. However, SEM images show that there was a relatively ductile fracture in the necking zones. Again, it was understood that these drops occurred

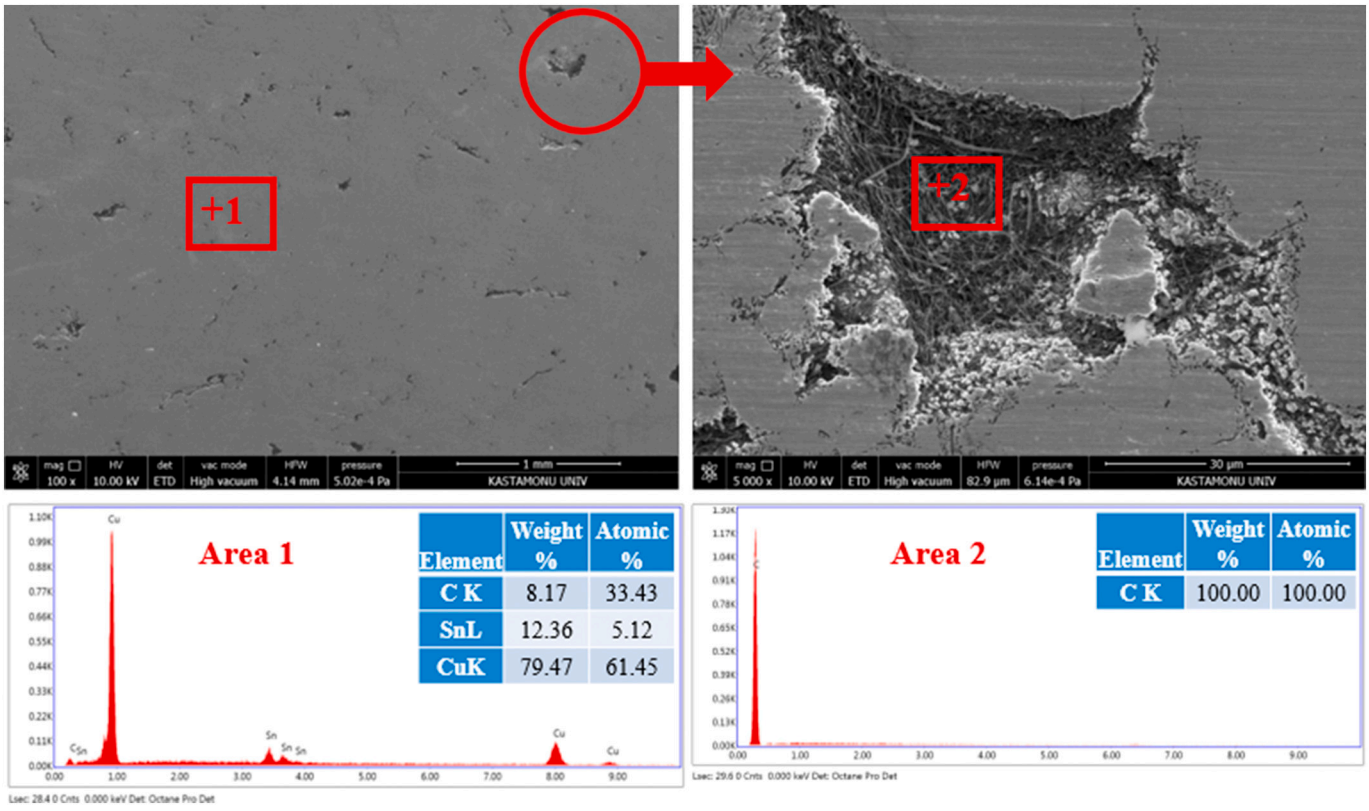

Fig. 4. SEM-EDS analysis of bronze- 0.50% CNF sample.

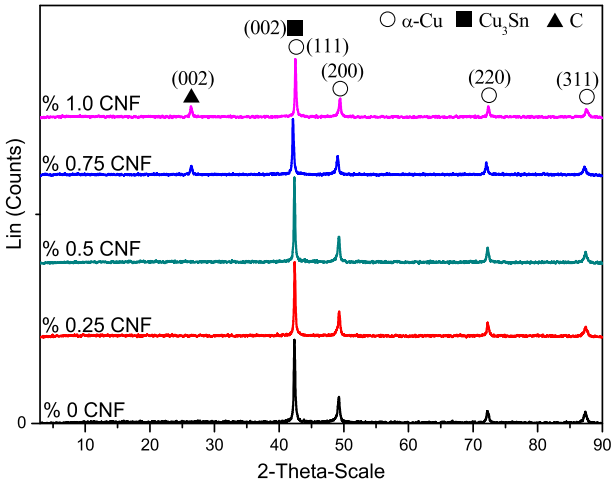

Fig. 5. XRD graph of the samples.

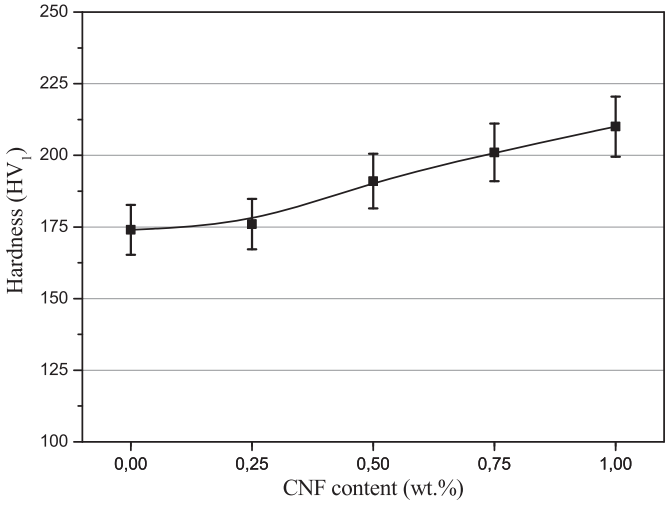

Fig. 6. Hardness of the samples as a function of CNF ratio.

Table 3
Experimental, theoretical, and relative densities of the samples.

Sample	Theoretical density (gr/cm^3)	Experimental density (gr/cm^3)	Relative density (%)
Bronze	8.69	8.60	99.0
Bronze-0.25% CNF	8.67	8.57	98.8
Bronze-0.50% CNF	8.65	8.55	98.8
Bronze-0.75% CNF	8.64	8.51	98.5
Bronze-1.00% CNF	8.62	8.48	98.4

in the diamond particles.

Fig. 12 shows the EDS analysis taken from the fracture surface of 1.00% CNF-reinforced bronze-CNF-diamond sample. EDS analysis was taken from three zones: matrix, diamond particle, and CNF. In zone 1, CNF was dense. Here, the amount of carbon was approximately 79.98 wt % which represents CNF. Zone 2 was taken from the diamond particle. Again, according to its analysis, the diamond was coated with titanium. EDS analysis of zone 3 represents the bronze matrix.

Fig. 13 shows friction coefficient-wear distance graph of the diamond-free samples. The average friction coefficients were 0.605, 0.576, 0.570, 0.434, and 0.363 for 0, 0.25, 0.50, 0.75 and 1.0% CNF reinforcements, respectively. The higher the CNF ratios got, the samples'

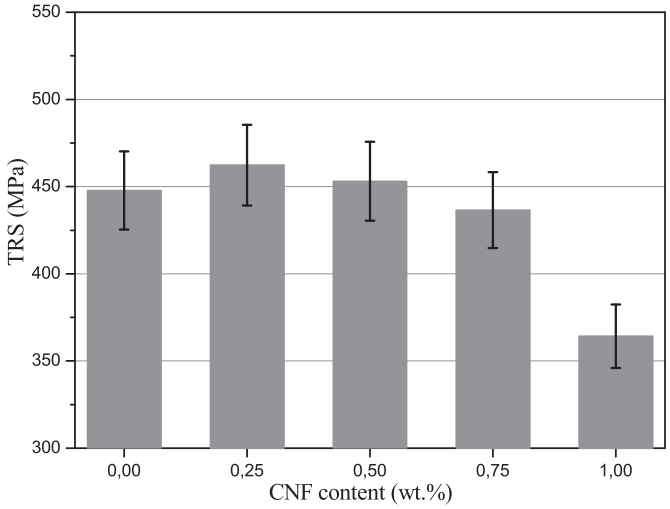

Fig. 7. Transverse rupture strengths as a function of CNF ratio of the samples.

friction coefficients dropped significantly. The CNFs caused a solid lubricant effect between the steel ball and the sample, thereby causing their samples friction coefficients to drop. Similar findings were observed in the Cu-Sn/CNT nanocomposites as well [26]. The wear rates of the samples dropped depending on increase in CNF ratio – as seen in Fig. 14 (except for 0.25% CNF). The wear rate for the non-reinforced bronze matrix was 7.6 × 10^{-4} mm^3 $(Nm)^{-1}$, whilst at CNF reinforcement of 1.0% it was 1.4 × 10^{-4} mm^3 $(Nm)^{-1}$. The CNFs caused dispersion strengthening in the bronze matrix, thereby lowering the wear rates.

Fig. 15 shows the SEM images and EDS analyses of the wear surfaces of non-reinforced and 1.0% CNF-reinforced samples. Deep wear marks and plastic deformation were observed in the non-reinforced sample (Fig. 15(a)). EDS analysis shows the presence of Cu, Sn, and O on the wear surface. Oxygen film creates a tribo-layer on the surface, thus lowering the friction coefficient. This film breaks down during wear and increases wear losses [27]. The matrix material (Cu—Sn) that breaks off from the surface adheres to the surface during wear. This wear mechanism belongs to the type of adhesive wear in question. EDS analysis of the surface of the 1.0% CNF-reinforced sample (Fig. 15(b)) shows that Cu, Sn and C were present on the sample's surface. Its wear mechanism turned into both adhesive and abrasive wear.

Fig. 16 shows the potentiodynamic polarization curves of the

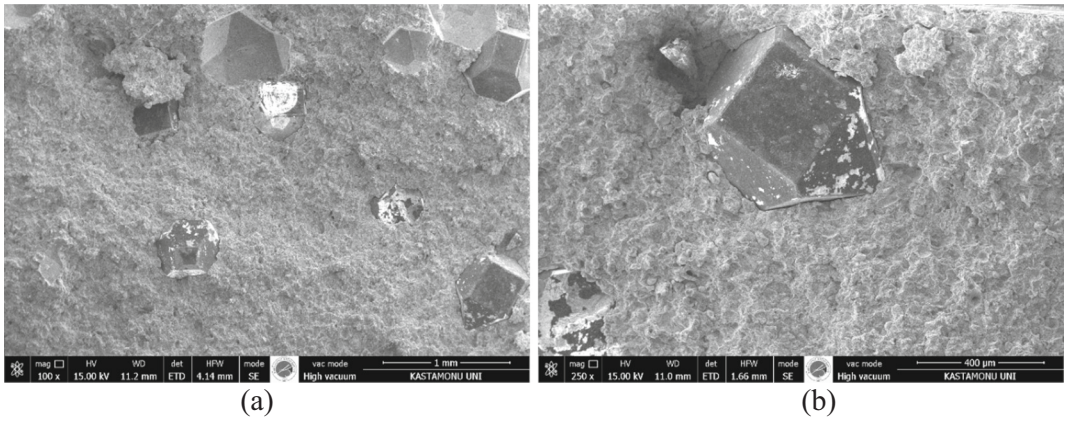

Fig. 8. The fracture surface of the non-reinforced sample (bronze-diamond): (a) x100 and (b) x250.

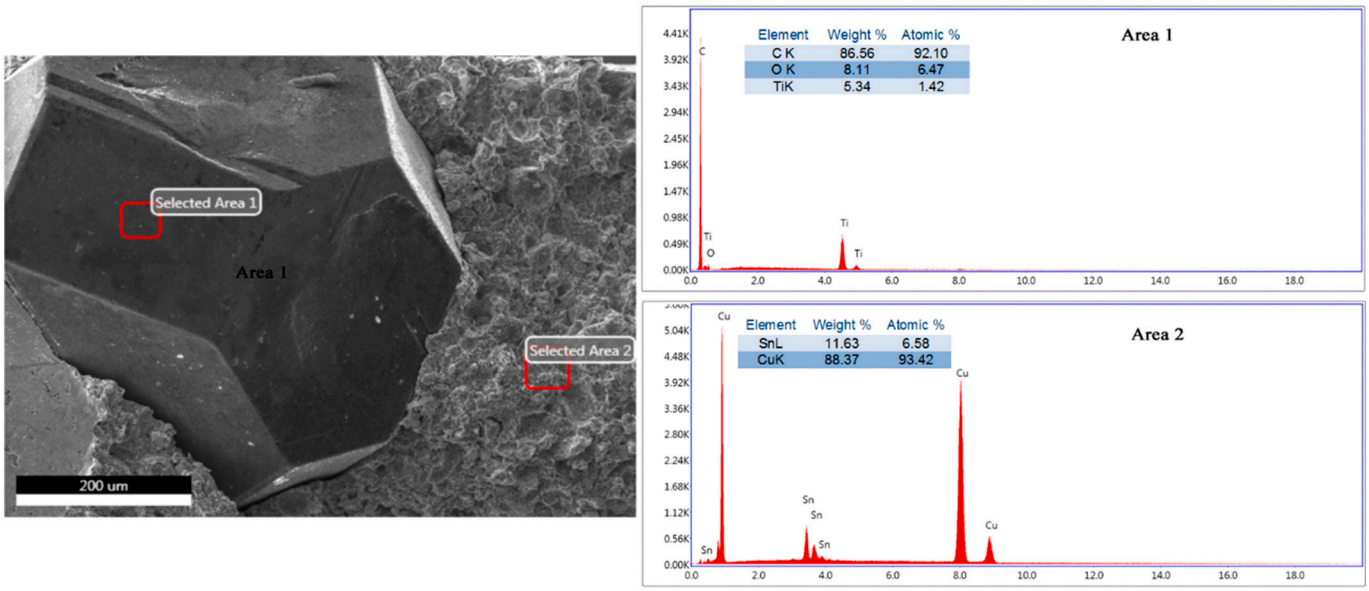

Fig. 9. EDS analysis of non-reinforced bronze-diamond samples.

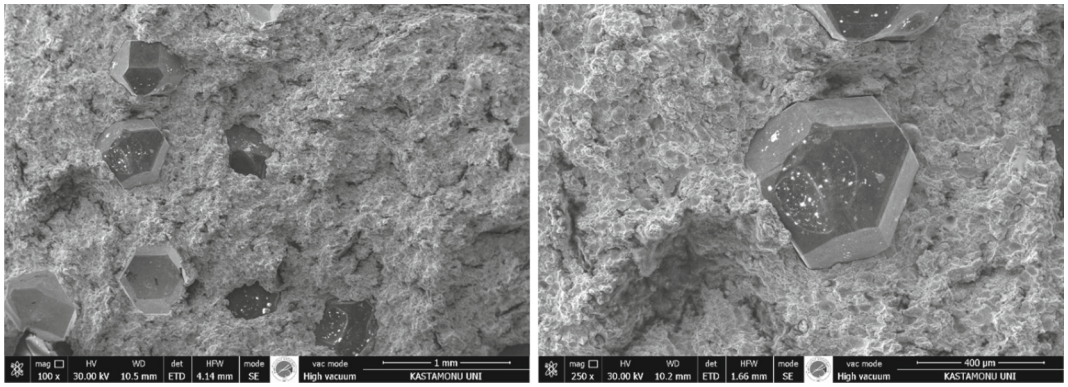

Fig. 10. The fracture surfaces of the bronze-0.25% CNF-diamond sample: (a) x100 and (b) x250.

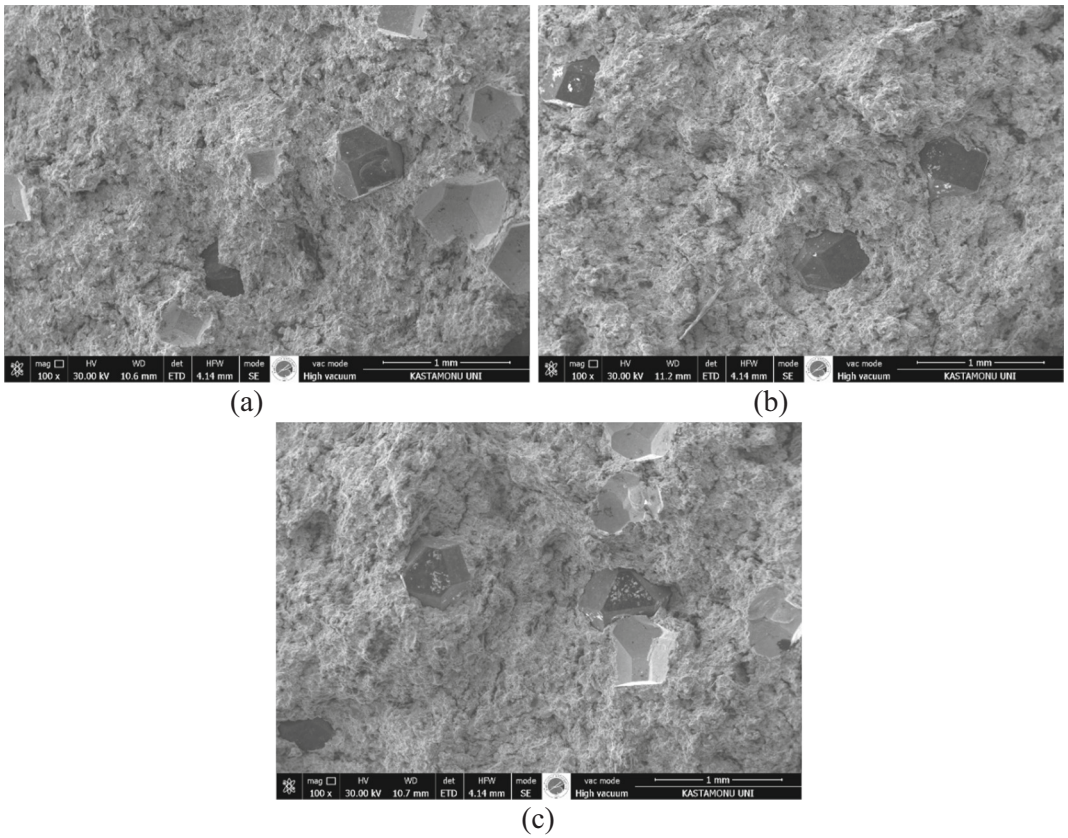

Fig. 11. Fracture surfaces of the samples at different CNF ratios: (a) 0.50% CNF, (b) 0.75% CNF and (c) 1.0% CNF.

samples. All corrosion measurements are summarised in Table 4. Corrosion potential (E_{corr}), anodic and cathodic Tafel slopes (β_a and β_c), alongside the corrosion rate and corrosion current (i_{corr}) were calculated from the Tafel curves. Corrosion resistance (R_p) was calculated using the Stern and Geary equation [28].

$$i_{corr} = \frac{\beta_a.\beta_c}{2.303 x R_p(\beta_a + \beta_c)}$$

The increase the ratio of carbon nanofibers led a negative increase in E_{corr}. Likewise, the increase in the ratio of carbon nanofibers caused the i_{corr} and the corrosion rates to rise. In other words, the addition of carbon nanofiber to the bronze matrix caused the corrosion resistance of bronze-carbon nanofiber materials to decrease. Other researchers have examined corrosion behaviours by adding carbon nanotubes to different metals. However, we have yet encountered any study that has specifically examined the corrosion of carbon nanofibers upon their being added to metal. Therefore, the findings were interpreted by comparing with other carbon nanoparticles. Aung et al. [29] added carbon nanotubes to magnesium and examined its effect on corrosion behaviour. They reported that carbon nanotubes increased corrosion rates of composite due to microgalvanic event. Turan et al. [30] examined the corrosion properties of magnesium-fullerene composites. As in the previous study, corrosion rates increased. The fact that corrosion rates increased with increasing ratio of carbon nanofiber due to the microgalvanic effect between bronze and carbon nanofibre in the present thesis study may be explained based on these studies. Fig. 17 shows the SEM-EDS analysis results of the surface of bronze and bronze-0.5% CNF samples after they were subjected to corrosion test. Na^+ and Cl^- ions

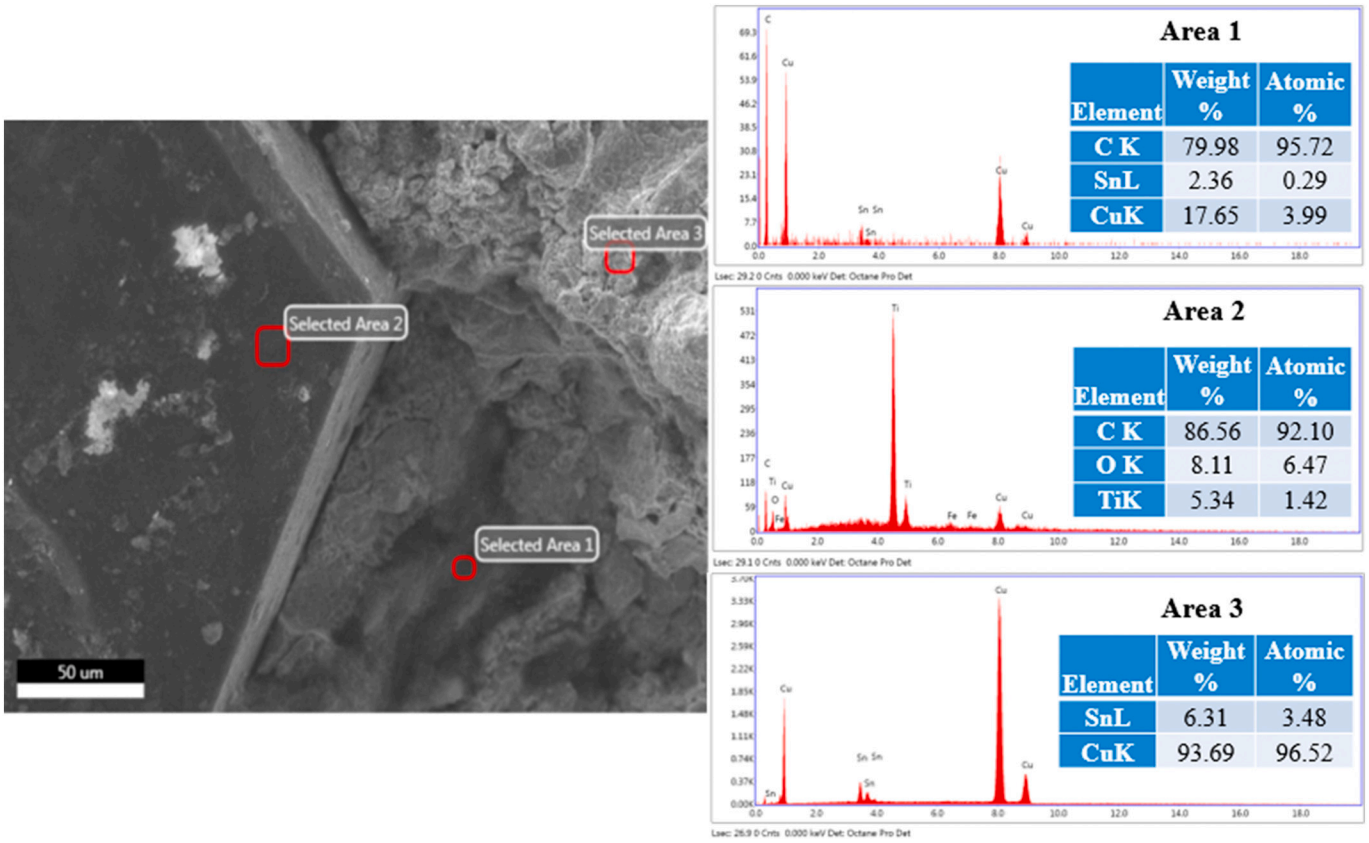

Fig. 12. EDS analysis of the 1.0%CNF-reinforced bronze-diamond sample.

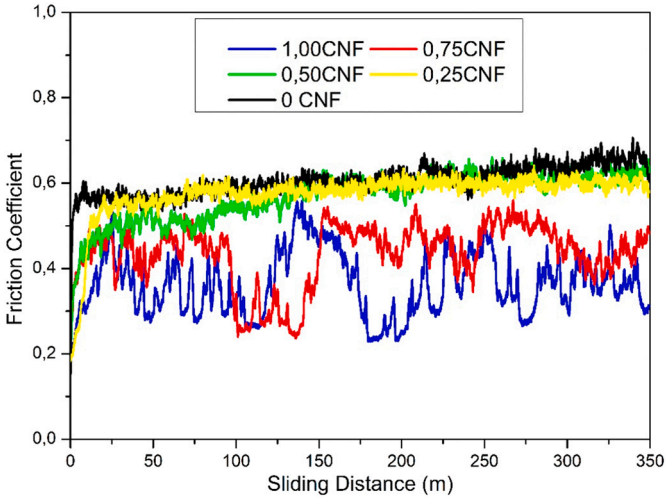

Fig. 13. Friction coefficient-wear distance graph.

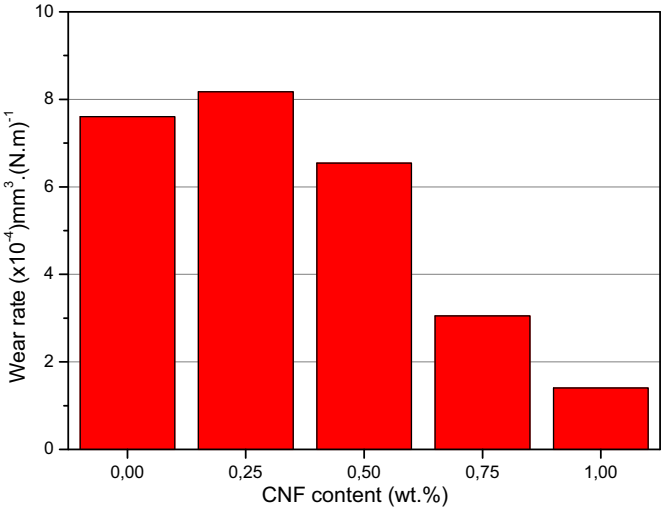

Fig. 14. Graph of wear rates.

were found in both the bronze sample and 0.5% CNF-reinforced sample they corroded during the electrochemical corrosion experiments. There were more ions in the 0.5% CNF-reinforced sample than the non-reinforced sample. Corrosion products were clearly visible in this sample after corrosion. Reinforced particles increased more cathodic corners as well. Moreover, the 0.5% CNF-reinforced sample indicates the presence of pitting corrosion caused by the absorption of chloride ions.

4. Conclusions

The following information, findings, and conclusions were obtained from this study, which aims to characterise carbon nanofibre-reinforced diamond cutting tools.

1) According to the optical images, there was a homogeneous dispersion at low ratios and a heterogeneous dispersion at higher ratios in the CNF matrix in all of the bronze-CNF-diamond samples. At higher CNF ratios, fibers clustered together in certain areas. XRD analyses indicated that α-Cu and Cu_3Sn phases formed in the non-reinforced bronze matrix, while phase C representing CNF formed in the CNF reinforcement alongside the α-Cu and Cu_3Sn phases.

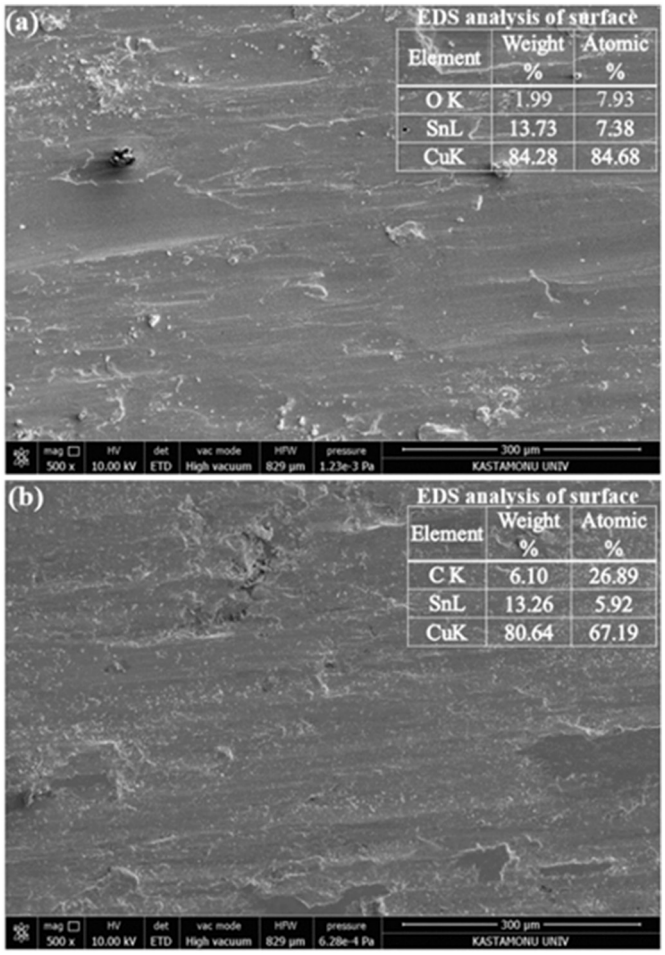

Fig. 15. SEM images and EDS analysis of wear surfaces: (a) Non-reinforced and (b) 1.0% CNF-reinforced.

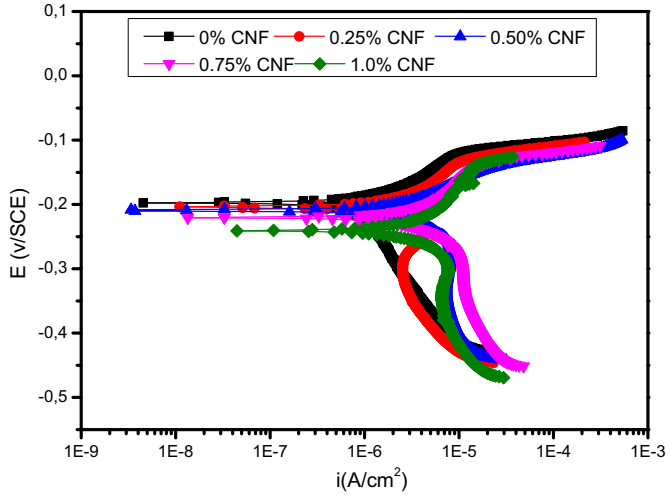

Fig. 16. Potentiodynamic polarization curves of the samples.

2) There was a slight drop in the experimental densities of the samples as the CNF ratio increased. A similar change was observed in their relative densities as well. The relative density was 99.0% in the non-reinforced sample and 98.4% in the 1.0% CNF-reinforced sample.
3) The matrices got harder the higher their CNF reinforcement ratios were. The highest hardness value was 210 HV_1 at 1.0% CNF reinforcement. This increase in hardness was caused by the free dispersion of CNF within the matrix.
4) The transverse rupture strength of the samples partially increased with the reinforcement of CNF. However, the non-homogeneous dispersion in increased CNF reinforcement ratio decreased the strength. According to the SEM images, fractures occurred mostly in the form of intergranular separation. However, there were relatively ductile fractures in the necking zones.
5) Depending on the increase in the ratio of CNF, both friction coefficients and wear rates decreased. Moreover, the adhesive wear mechanism prevailed in the non-reinforced sample, while both adhesive and abrasive wear prevailed in the CNF- reinforced sample.

Table 4
Electrochemical results of the samples.

Samples	E_{corr} (mV)	I_{corr} (μAcm^{-2})	β_a ($e^{-3}V$/decade)	β_c ($e^{-3}V$/decade)	CR (e^{-3}mpy)	Rp ($e^{-3}\Omega cm^2$)
0% CNF	−197	0.062	17.4	16.4	47.29	59.13
0.25% CNF	−204	0.323	23.9	23.2	246.7	15.83
0.50% CNF	−209	0.890	21.0	29.2	679.2	5.96
0.75% CNF	−221	1.040	24.6	22.3	796.0	4.88
1.0% CNF	−241	1.160	39.3	39.6	886.1	7.38

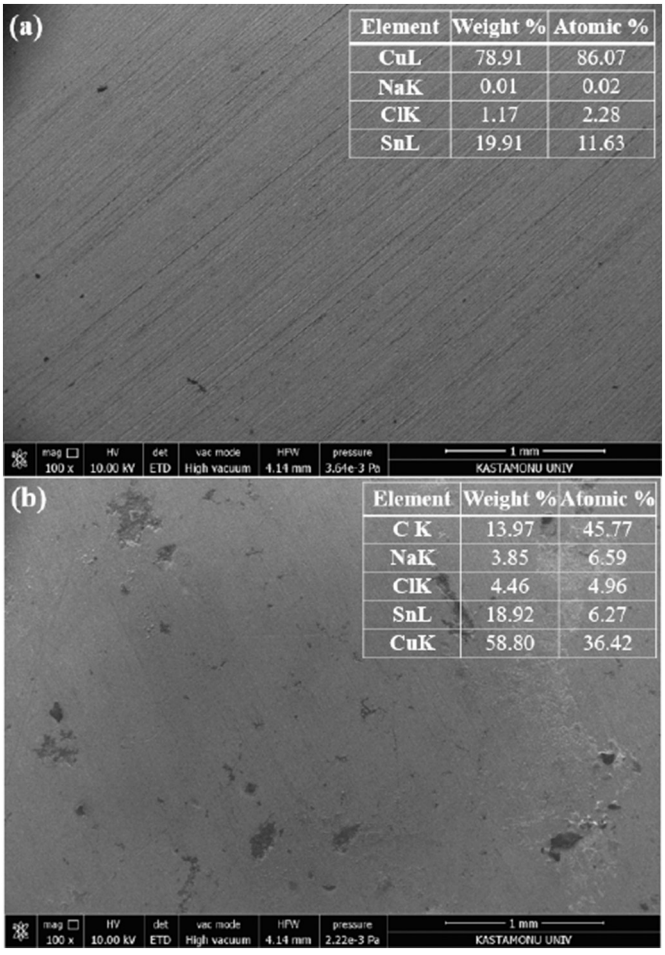

Fig. 17. SEM-EDS of the sample surfaces after corrosion: (a) bronze and (b) bronze- 0.50% CNF.

6) According to the results of the corrosion test, the corrosion rates of bronze-CNF samples increased with increased ratio of CNF. Likewise, the corrosion resistance of the samples decreased with increase in CNF.

CRediT authorship contribution statement

Serkan Islak conceived and designed the experiments; Naser Matoug Emhmed Abouacha and Cihan Özorak performed the experiments; Serkan Islak, Vahdettin Koç, Özkan Küçük and Uğur Çalıgülü analysed the data; Serkan Islak wrote the paper.

Declaration of competing interest

There are no conflicts of interest for all listed authors.

Acknowledgments

We would like to thank Kastamonu University Scientific Research Projects Unit for their financial support on project numbered KÜBAP 01 / 2017-49.

References

[1] J. Konstanty, Powder Metallurgy Diamond Tools, in: The Metal Powders Technology Series, Elsevier Ltd, 2005.
[2] S. Islak, Effect of Sintering Parameters on Sawing Performance of Marble Cutting Tools With Carbide, Firat University, Elazig, Turkey, 2012. Doctora Thesis.
[3] F. Chen, Z. Yan, Z. Liu, Y. Long, N. Fu, F. Zhang, B. Liu, Y. Liu, Preparation and properties of Al2O3-reinforced cu-ni-sn metallic matrix for applications in diamond-cutting tools, Diam. Relat. Mater. 109 (2020), 108025, https://doi.org/10.1016/j.diamond.2020.108025.
[4] Z. Su, S. Zhang, J. Wu, L.L. Liu, Cutting performance evaluation of nickel-plated graphite fe-based diamond saw blades, Diam. Relat. Mater. 114 (2021), 108344, https://doi.org/10.1016/j.diamond.2021.108344.
[5] H.X. Hu, W. Chen, C. Deng, Effect of Fe prealloyed powder and the sintering process on the matrix properties of impregnated diamond bits, J. Mater. Res. Technol. 12 (2021) 150–158, https://doi.org/10.1016/j.jmrt.2021.02.070.
[6] H.M. Soltani, M. Tayebi, Determination of wear parameters and mechanisms of diamond/copper tools in marble stones cutting, Int. J. Refract. Met. Hard Mater. 87 (2020), 105172, https://doi.org/10.1016/j.ijrmhm.2019.105172.
[7] E. Cygan-Baczek, P. Wyzga, S. Cygan, P. Bala, A. Romanski, Improvement in hardness and Wear behaviour of iron-based Mn–Cu–Sn matrix for sintered diamond tools by dispersion strengthening, Materials 14 (7) (2021) 1774, https://doi.org/10.3390/ma14071774.
[8] E. Çelik, A.K. Aslan, Effect of post-heat treatment on microstructure and mechanical properties of cu-fe-co powder alloy fabricated by hot pressing, Arch. Metall. Mater. 63 (1) (2018) 371–377, https://doi.org/10.24425/118950.
[9] E. Çelik, Investigation of hot pressing charesteristisc of mecanically alloyed FeCuNiSnPMoMn alloy used as Co alternative, Sci. Eng. J. Firat Univ. 29 (1) (2017) 145–150.
[10] W. Li, J. Zhan, S. Wang, H. Dong, Y. Li, Y. Liu, Characterizations and mechanical properties of impregnated diamond segment using cu-fe-co metal matrix, Rare Metals 31 (1) (2012) 81–87, https://doi.org/10.1007/s12598-012-0467-x.
[11] B. Bulut, O. Gunduz, M. Baydogan, E.S. Kayali, Determination of matrix composition for diamond cutting tools according to the hardness and abrasivity properties of rocks to be cut, Int. J. Refract. Met. Hard Mater. 95 (2021), 105466, https://doi.org/10.1016/j.ijrmhm.2020.105466.
[12] E. Çelik, S. Islak, C. Ilkiliç, Production of matrices with molybdenum as an alternative to matrices with cobalt in diamond cutting tools, Mater. Tehnol. 48 (6) (2014) 881–884.
[13] M. Zhang, W. Zhang, Y. Liu, B. Liu, J. Wang, FeCoCrNiMo high-entropy alloys prepared by powder metallurgy processing for diamond tool applications, Powder Metall. 61 (2) (2018) 123–130, https://doi.org/10.1080/00325899.2018.1429044.
[14] M. Zeren, S. Karagöz, Sintering of polycrystalline diamond cutting tools, Mater. Des. 28 (3) (2007) 1055–1058, https://doi.org/10.1016/j.matdes.2005.09.018.
[15] D. Kir, S. Islak, H. Çelik, E. Çelik, Effect of the cBN content and sintering temperature on the transverse rupture strength and hardness of cBN/diamond cutting tools, Sci. Sinter. 44 (2) (2012) 235–243, https://doi.org/10.2298/SOS1202235K.
[16] S. Islak, D. Kir, H. Çelik, Investigation of the usability of cubic boron nitride cutting tools as an alternative to diamond cutting tools, Arch. Metall. Mater. 58 (4) (2013) 1119–1123, https://doi.org/10.2478/amm-2013-0135.
[17] S. Islak, H. Çelik, Effect of sintering temperature and boron carbide content on the wear behavior of hot pressed diamond cutting segments, Sci. Sinter. 47 (2) (2015) 131–143, https://doi.org/10.2298/SOS1502131I.
[18] J.Y. Lim, S.I. Oh, Y.C. Kim, K.K. Jee, Y.M. Sung, J.H. Han, Effects of CNF dispersion on mechanical properties of CNF reinforced A7xxx nanocomposites, Mater. Sci. Eng. A 556 (2012) 337–342, https://doi.org/10.1016/j.msea.2012.06.096.
[19] J.F. Silvain, C. Vincent, J.M. Heintz, N. Chandra, Novel processing and characterization of Cu/CNF nanocomposite for high thermal conductivity applications, Compos. Sci. Technol. 69 (14) (2009) 2474–2484, https://doi.org/10.1016/j.compscitech.2009.06.023.
[20] H. Kwon, H. Kurita, M. Leparoux, A. Kawasaki, Carbon nanofiber reinforced aluminum matrix composite fabricated by combined process of spark plasma sintering and hot extrusion, J. Nanosci. Nanotechnol. 11 (5) (2011) 4119–4126, https://doi.org/10.1166/jnn.2011.3866.
[21] J. Dwan, Fracture toughness determination of diamond impregnated PM cobalt, Ind. Diam. Rev. 1 (2007) 33–36.
[22] M. Filgueira, D.G. Pinatti, In situ diamond wires: part II. The bronze 4 wt.% diamond composite cutting rope, J. Mater. Process. Technol. (1-3) (2003) 132–137, https://doi.org/10.1016/S0924-0136(02)00450-8.
[23] X. Liang, C. Jia, K. Chu, H. Chen, J. Nie, W. Gao, Thermal conductivity and microstructure of Al/diamond composites with ti-coated diamond particles consolidated by spark plasma sintering, J. Compos. Mater. 46 (9) (2012) 1127–1136, https://doi.org/10.1177/0021998311413689.
[24] D. Egan, J.A. Engels, The use of coated diamonds in diamond impregnated tools, Ind. Diam. Rev. 4 (04) (2004) 34–38.
[25] X. Xu, X. Tie, H. Wu, The effects of a ti coating on the performance of metal-bonded diamond composites containing rare earth, Int. J. Refract. Met. Hard Mater. 25 (3) (2007) 244–249, https://doi.org/10.1016/j.ijrmhm.2006.06.002.
[26] H.M. Mallikarjuna, K.T. Kashyap, P.G. Koppad, C.S. Ramesh, R. Keshavamurthy, Microstructure and dry sliding wear behavior of cu-sn alloy reinforced with multiwalled carbon nanotubes, Trans. Nonferrous Metals Soc. China 26 (7) (2016) 1755–1764, https://doi.org/10.1016/S1003-6326(16)64269-3.
[27] S. Islak, Ö. Eski, V. Koç, C. Özorak, Wear properties and synthesis of CrFeNiMoTi high entropy alloy coatings produced by TIG process, Indian J. Eng. Mater. Sci. 27 (3) (2020) 659–664.
[28] M. Stern, A.L. Geary, Electrochemical polarization I.A theoretical analysis of the shape of polarization curves, J. Electrochem. Soc. 104 (1) (1957) 56–63, https://doi.org/10.1149/1.2428496.
[29] N.N. Aung, W. Zhou, C.S. Goh, S.M.L. Nai, J. Wei, Effect of carbon nanotubes on corrosion of Mg–CNT composites, Corros. Sci. 52 (5) (2010) 1551–1553, https://doi.org/10.1016/j.corsci.2010.02.025.
[30] M.E. Turan, Y. Sun, Y. Akgul, Mechanical, tribological and corrosion properties of fullerene reinforced magnesium matrix composites fabricated by semi powder metallurgy, J. Alloys Compd. 740 (2018) 1149–1158, https://doi.org/10.1016/j.jallcom.2018.01.103.